PRELIMINARY THERMAL ANALYSIS OF A MARS SAMPLE RETURN EARTH ENTRY VEHICLE

Ruth M. Amundsen, John A. Dec, Robert A. Mitcheltree, Michael C. Lindell, Robert A. Dillman
National Aeronautics and Space Administration
Langley Research Center
Hampton VA 23681-2199

ABSTRACT

Thermal analysis of a vehicle designed to return samples from another planet, such as the Earth Entry vehicle for the Mars Sample Return mission, presents several unique challenges. The scientific purpose of a sample return mission is to return samples to Earth for detailed investigation. The Earth Entry Vehicle (EEV) must contain the samples after they have been collected and protect them from the high heating rates of entry into the Earth's atmosphere. This requirement necessitates inclusion of detailed thermal analysis early in the design of the vehicle. This paper will describe the challenges and solutions for a preliminary thermal analysis of an Earth Entry Vehicle. The primary challenges included accurate updates of model geometry, applying heat fluxes that change with position and time during exo-atmospheric cruise and entry, and incorporating orthotropic material properties. Many different scenarios were evaluated for the exo-atmospheric cruise to attain the desired thermal condition. The severity of the heat pulse during entry and the material response led to some unique modeling solutions. Overall, advanced modeling techniques and mathematical solutions were successfully used in predicting the thermal behavior of this complex system.

INTRODUCTION

The purpose of the Mars Sample Return Mission is to return a sample of Martian material to Earth so that it may be studied here. The Earth Entry Vehicle (EEV) to accomplish the return of the samples to the Earth's surface must be robust and extremely reliable. Some of the reasoning behind design of the vehicle is discussed in an earlier publication on a similar design.[1] This paper will describe the thermal modeling and design of one possible design of an EEV (the November 1999 reference concept) of the many designs under evaluation.

The design of a Mars Sample Return Earth Entry Vehicle has many unique finite element modeling challenges associated with it, both of a structural and thermal nature. The purpose of the Earth Entry Vehicle is to protect Mars samples from the mechanical and thermal environment encountered during Earth entry and landing, while assuring sample containment. The science requirement on thermal design is that the returned samples will not experience a temperature over 50°C throughout all mission phases. The system requirement is that no component should go outside its survival temperature range during cruise, or outside its operational temperature range during operation.

The EEV expected lifetime of about three years can be separated into several distinct thermal phases. For the first several years, it would be attached to the spacecraft during the planetary travel and sample collection intervals. Several days before arrival into the Earth's atmosphere, the EEV would be spin-ejected from the spacecraft and begin the exo-atmospheric cruise portion of the journey. The entry into Earth's atmosphere would be the third phase, with aerodynamic heating boundary conditions very different than the first two phases. The fourth phase would be equilibration of the EEV to ambient temperature conditions on the Earth's surface after landing. Only the last three phases are discussed in this paper.

This paper will describe the challenges inherent in this analysis, and the solutions employed. One challenge is keeping up with rapid design changes and rapid trajectory changes. In order to be useful, the analysis must be able to respond with quick answers to "what-if"

scenarios regarding geometry or trajectory changes. Another challenge is defining the exterior properties of the vehicle so that appropriate temperatures are maintained both while attached to the spacecraft, and after separation. The cruise after separation is in a hyperbolic orbit, which complicates the simulation. The heat pulse at entry challenges both the mesh density and the thermal solver. The material responses (such as pyrolysis) during the heat pulse must be taken into consideration. Finally, three-dimensional orthotropic properties on these randomly oriented components are a challenge to incorporate.

The thermal analysis results are valuable for several reasons. First, the thermal environment experienced by the returned samples can be predicted, and if not acceptable for science reasons, design modifications can be made. The thermal history of each material in the vehicle design can also be compared to its survival range, to ensure that all designed materials are adequate. The thermal predictions for operational mechanical and electronic components can be used to ensure they remain within their acceptable thermal range. Another use for the thermal predictions is to predict thermal stresses and deflections in the vehicle. The exo-atmospheric phases involve cold temperatures and slow changes, as well as a moderate gradient across the vehicle. The entry phase involves very rapid changes in temperature and gradients across the vehicle. Each thermal case can be used for structural analysis of the vehicle, to determine if unacceptable stresses or deflections are encountered.

DESIGN DESCRIPTION

This particular preliminary design of an EEV is shown in Figure 1. This is the November 1999 reference EEV concept[2]. This is an on-going design process, and both the design and associated analysis are expected to change. The forebody thermal protection system (TPS) is PICA-15, a material developed at NASA Ames. The afterbody TPS is SIRCA. The substructure is carbon-carbon. The wing foam is a low density but stiff carbon foam. The samples are held within an orbiting sample canister (OS), and the OS is enclosed within a containment vessel (CV). The CV/OS is within an impact sphere filled with energy absorbing material. The impact sphere is protected at the stagnation point by a nosecap of carbon-phenolic and a fiberform insulator. The entire forebody is covered with a 3-layer multi-layer insulation blanket (MLI) which extends back to the spin-eject ring on the aft side.

During the 4-day exo-atmospheric cruise after separation, the spin stabilized EEV is in a hyperbolic orbit ending at atmospheric entry. The solar angle during this cruise is at roughly 45° off the nose, such that the solar flux falls only on the forebody.

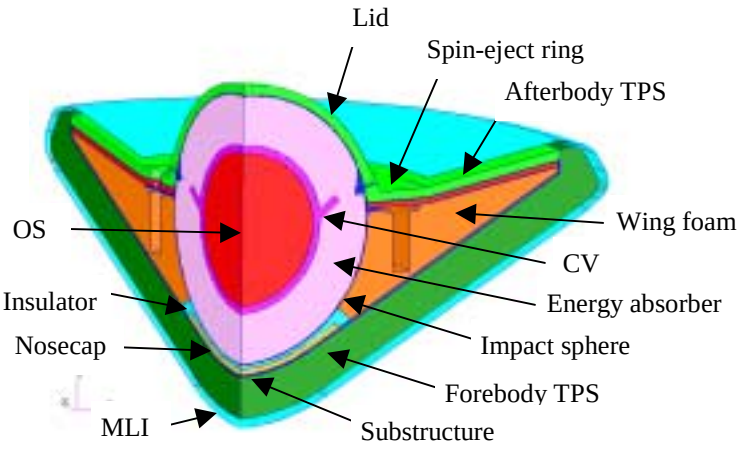

Figure 1. EEV quarter model geometry.

THERMAL MODELING

Geometry

One challenge in modeling an Earth Entry Vehicle (EEV) during preliminary design is tracking frequent design changes. It is important to have an analysis method that allows quick evaluation of potential design modifications. The method employed in this analysis is to import design geometry directly from the computer-aided design (CAD) software Pro/Engineer[3] into the modeling software MSC/PATRAN[4*]. This geometry can be directly meshed to create the analysis model. In some cases, a design modification can be evaluated by simply altering a material or boundary condition in the model. For a more substantial design change, a new geometry or part must be imported. Even when a new geometry is imported, re-analysis can be relatively fast since all the boundary conditions and materials applied to the geometry can be re-used. In this manner, design changes and updates can be rapidly incorporated, rather than necessitating long periods of manual dimension input to the modeling software.

The geometry comes into PATRAN with major parts separated into groups. For initial analysis, minor parts such as bolt holes and bolts were disregarded. As the

---

[*] The use of trademarks or names of manufacturers in this report is for accurate reporting and does not constitute an official endorsement, either expressed or implied, of such products or manufacturers by the National Aeronautics and Space Administration.

analysis becomes more sharply defined, these parts can be retained and incorporated in the analysis. The thermal solver is currently PATRAN Thermal 9.0. All thermal models are only one-quarter of the vehicle since it is symmetric (beacon assemblies and other non-symmetric items such as bolts have not yet been added). A study was performed to evaluate doing the analysis in this initial phase with a 2D axi-symmetric model. 2D axi-symmetric and 3D quarter models were developed, and solved for the same boundary conditions. The 2D axi-symmetric model did not give a faster solution time, and is actually more time-consuming to create from the CAD geometry. Thus, the 3D quarter models were used for the remainder of the work. Three-dimensional models also allow capturing the behavior of non-symmetric components such as bolts, push-pads and beacons later in the process.

The modeling of orbital fluxes could not be done using PATRAN, so the Thermal Synthesizer System (TSS)[5] software was used. TSS was used because of its capability to handle a hyperbolic orbit analysis via input of discrete trajectory points. TSS does not currently have geometry import capability from Pro/Engineer. Thus, this model was developed independently. This was not a large effort since only the main exterior shapes of the vehicle need to be captured. In order to allow rapid response to design changes, the model was built using variables. By changing one or many of only five variables, the entire outer shape of the vehicle could be modified.

Model Phases

The modeling is separated into four distinct phases: cruise with the spacecraft, post-separation exo-atmospheric cruise, atmospheric entry to landing, and post-landing. The different phases of analysis have very different timelines as well as very different heating rates. The exo-atmospheric cruise portion may last for several days, whereas the heat pulse at entry is less than a minute. The configuration on the spacecraft is very different than any other, since it is held in place by rigid mounts, has a limited view of space, and has extra insulation that is not carried with the vehicle.

The exo-atmospheric cruise phase and the entry phase have similar boundary conditions in that both have heat fluxes, convection and radiation applied to the entire exterior of the vehicle. However, in the entry phase the heat pulse is severe enough that a very fine mesh must be used. The required density of the mesh is determined by the capability of the solver to handle the element size and still come to a converged solution. This model is a transient that only lasts for 473 seconds, so the solution time can be kept reasonable even with a very fine mesh. If that dense a mesh were used on the exo-atmospheric case, where the transient is four days and there are many parametric cases to be run, solution time would be excessive. Thus, the same geometry and materials are shared between these two models, but the meshing is different. Boundary condition transfer between the phases is straightforward since the identical geometry is used for each mesh. By applying boundary conditions to the geometry, rather than the mesh, the evaluation of different mesh densities is facilitated. Temperatures are transferred between the model phases by mapping the results back to the geometry, independent of the differing meshes.

The post-landing model is very similar to the exo-atmospheric case in that it is a long-term transient (24 hours) where a coarse mesh is acceptable. Thus, the same geometry and mesh as the exo-atmospheric case are used, although most boundary conditions are different. The post-landing state of the vehicle presents a challenge since there are many possible alternatives. The vehicle may be in any one of many possible orientations, yielding a host of potential air convection and ground contact possibilities. The range of possible ground material compliance is wide, which can vary the amount of the vehicle in contact with the ground. Also, the time interval before the vehicle is located is variable, and the ambient temperature and wind conditions are difficult to predict. Thus, several general cases must be run to bound the problem.

Heat Flux Boundary Conditions

Another common change that must be anticipated when performing detailed thermal analysis early in the design of the vehicle is modifications to the trajectory and heating rates. When the trajectory changes, both the exo-atmospheric cruise and entry heating loads are affected. Rapid evaluation of the changes is beneficial in allowing final trajectory design. Heat flux boundary conditions are applied via an external text file, so that changes to the trajectory and heating rates can be easily made via substitutions in that file.

The orbital heat loads during the exo-atmospheric phase must be calculated for a hyperbolic orbit. Many of the available orbital/radiation analysis tools do not handle hyperbolic orbits. A methodology was developed using the Thermal Synthesizer System software to analyze and visualize the incoming hyperbolic trajectory. This method allowed quick calculation of orbital heating on the exterior of the vehicle, from both solar and planetary sources, for a variety of vehicle shapes and trajectory definitions. Figure 2 shows an example TSS model with heat fluxes on the vehicle surface. Visual verification of the trajectory, orientation and exterior

heat fluxes is a key factor in the analysis. The heat loads from this analysis are automatically captured in a single file, thus simplifying the incorporation of this data into the overall thermal analysis and the evaluation of several trajectories for a single vehicle design. The vehicle is spinning at 2 rpm, so calculated fluxes were averaged around the vehicle to account for the spin. The averaged fluxes were applied to the PATRAN model via the text output file from TSS.

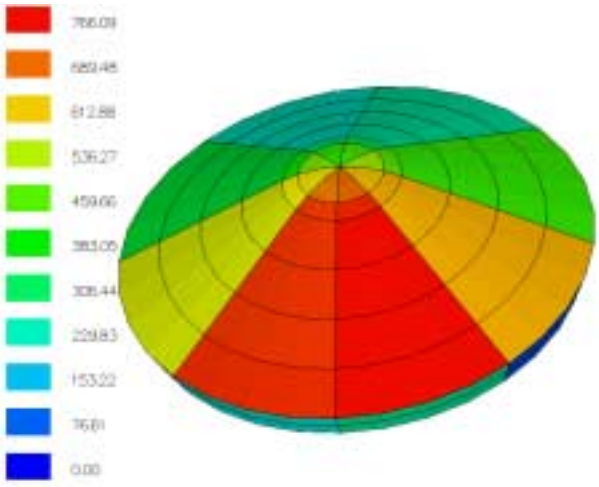

Figure 2. Solar fluxes calculated by TSS (W/m2).

The heat pulse of an earth entry must be modeled precisely in order to fully understand its effect on the subsequent thermal behavior. The aerodynamic heating is a function not only of time, since velocity and atmosphere are both altering radically with time, but also of the position on the vehicle surface. Several unique methods were found to incorporate an accurate representation of this heating into the model. Aeroheating predictions on the forebody varied both in time and spatial position. To capture this on the forebody, the stagnation point heating (convective plus radiative) as a function of time (Figure 3) was multiplied by the spatial factor on the forebody as function of radial distance (Figure 4). This spatial factor, the drop-off in heating away from the centerline, was thus assumed to be constant with time, when it actually changes with time. This will be improved in later modeling, but since the factor is only important over a short time period (about 40 seconds), the approximation is good enough for preliminary design evaluation. On the afterbody, due to the difficulty inherent in afterbody CFD predictions, a constant spatial factor was used. This factor was 4% of the forebody stagnation point heating timeline multiplied by an uncertainty factor of 3. Thus, 12% of the stagnation point flux in Figure 3 was used over the afterbody at each point in time. The heating data when applied in this manner does not account for the charring effects of the ablative TPS materials. In order to correct this, the thermal predictions for TPS sizing at the stagnation point (done by YK Chen at NASA Ames) were used as a baseline for comparison, as discussed in the Correlation to FIAT Model section.

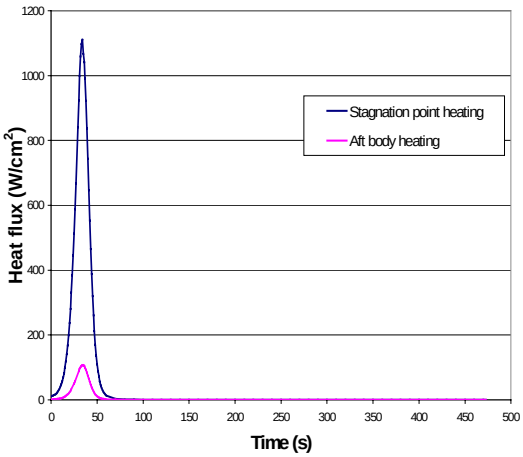

Figure 3. Heat flux versus time on EEV.

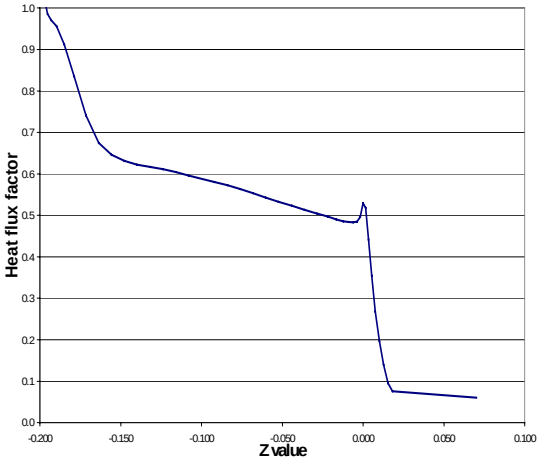

Figure 4. Spatial factor on forebody.

Other Boundary Conditions

Contacts between the components are modeled via pseudo-convection boundary conditions. All components are connected via a 0.13-mm adhesive bond, which gives a contact conductance of 1500 W/m^2K. This bondline may be thickened in later designs, so several parametrics were run with lower contact conductances -- the variation had little effect. The only unbonded attachment is the OS within the CV; since this is a loose contact connection it is rated at a lower conductance of 100 W/m^2K.

Current assumptions for the exo-atmospheric model include an EEV temperature at release of –80°C. This value is not critical to later operations, since regardless

of the release temperature, the EEV will come to the same equilibrium during the four-day cruise before Earth entry. During exo-atmospheric cruise there is an MLI blanket in place that extends over the entire forebody and afterbody up to the spin-eject ring. There is no blanket over the spherical aft lid or the flat disk where the spin-eject ring mounts. The effective emissivity (ε*) of the blanket, driven by JPL heater power limits, is 0.03. The exterior of the MLI, and the non-insulated portions of the vehicle, radiate to deep space and absorb solar fluxes as determined by their optical properties. Several optical properties were evaluated, as described in the Parametric Studies section. The solar orientation during the four-day cruise varies from 45.2 degrees off the nose at separation to 47.5 degrees off the nose at entry.

The entry phase model includes the heat flux loads as discussed above. It also includes radiation and nominal convection to the atmosphere. The atmospheric temperature as a function of time was derived from the altitude using a GRAM-95 model. The convection to the atmosphere uses a convective h value that is currently a very low approximation. After additional CFD runs determine the extent of turbulence and local conditions, this number can be better defined. Radiation to the atmosphere is the driver in decreasing EEV surface temperatures. It is assumed that the MLI breaks away rapidly (as designed), so the surface emissivity used (0.8) is for the PICA itself.

The post-landing model includes the initial temperature from the entry phase, as well as radiation and convection to a 25°C ambient. All assumptions are designed to be conservative in the sense of predicting the warmest possible OS temperature. Even with the conservative assumptions, the OS does not go above its 50°C science limit.

Transfer between Phases

Transfer of temperatures between the model phases is accomplished by interpolating the temperatures from one phase's mesh on to the next phase model. This is easily done within PATRAN, and this interpolated temperature forms the initial temperature boundary condition for the next phase.

Material Properties

Material properties for the TPS materials were taken from the TPSX software[6], with some modifications by NASA Ames personnel. Carbon-carbon and other composite properties were from Langley reports.[7,8] Other material properties were from vendor literature, from the PATRAN Thermal materials database, and from independent calculations. All material properties with substantial temperature variation were input as tables versus temperature.

Initially the materials were modeled as isotropic. This is not a valid assumption for some of the fiber-based materials such as the forebody TPS (PICA) and the carbon-carbon structure. For these orthotropic materials, through-thickness and in-plane conductivity properties were added. In general, the in-plane conductivity is appreciably higher than the through-thickness property due to the in-plane orientation of the fibers. Thus, this model refinement makes a substantial difference in the heat flow and overall thermal behavior.

The difficulty in adding the orthotropic properties is that the materials are not oriented in any constant axis of the model. On the forebody TPS spherical cap, for example, the direction of the through-thickness property is changing continuously in two directions of rotation. In PATRAN, the orientation of an orthotropic material is defined by three Eulerian rotation angles about the x, y and z axes. Since the Eulerian rotation of the material is different at each point on most of these components, a spatial field was used to define these rotations. By making the spatial field a specific function of two spatial variables, the field could be defined as exactly the Eulerian rotation necessary to bring the material axes into the correct orientation at each position. Each field was written as an equation of the following form:

$$\phi = \sin^{-1}\left(\frac{Z}{R}\right) * \cos\left(\tan^{-1}\left(\frac{X}{Z}\right)\right) \qquad (1)$$

where ϕ is the material rotation around the x-axis, R is the component radius at that point, and X and Z are the location in the x and z axes. This equation was varied for the conical parts, as well as for parts such as the lid where the curvature was inverted (concave rather than convex). Each of the curved orthotropic components had x-rotation and z-rotation defined in this manner (no rotation around y since it was the axis of symmetry). The materials affected were PICA, SIRCA, carbon-carbon, fiberform, and graphite-polyimide. Changes due to refining the material properties in this way are shown in the results sections.

EXO-ATMOSPHERIC PHASE RESULTS

Parametric Studies

After separation from the spacecraft, the EEV comes to equilibrium within several hours, and there are no major changes until the vehicle has a substantial view of Earth (in the last hour). Thus, the thermal behavior is constant over a majority of the time. This being the

case, this model was usually run as steady state in order to quickly evaluate the effect of different boundary conditions and materials. Once a set of materials and coatings were selected, this model was run as a transient to evaluate the real-time behavior.

The thermal response during exo-atmospheric cruise is almost completely driven by the orientation of the EEV with respect to the sun, and by the coatings and coverings on the exterior of the EEV. Several parametric cases were run to determine an optimum set of properties. Currently, it is assumed that MLI will be needed on the exterior of the EEV in order to minimize the heater power needed while attached to the spacecraft. The drivers on selecting exterior properties are as follows. The OS must be kept at a reasonably low temperature, well below the limit of 50°C. The adhesive bondlines should all be kept above –80°C to maintain structural integrity. The beacon assembly, which is located within the wing foam, should be kept above –40°C. In order to facilitate flight testing, it is desired that most structural components be kept as near room temperature as possible.

Since there is MLI on the forebody that limits the heat input from solar flux, and there is no solar flux impinging on the unprotected afterbody, the EEV temperature tends to run colder than desired. To mitigate this, materials with relatively high α and low ε for the MLI exterior were examined from several sources[9,10]. This property of the MLI will tend to increase the heat input to the vehicle and raise the overall temperature. Examples of materials to achieve these properties are anodized titanium foil, the GSFC dark mirror coating (SiO-Cr-Al), black irridite, germanium foil, chromium foil, and striping of these materials with conventional ones. On the afterbody, there are no solar fluxes, so the α value is meaningless until the EEV is very close to Earth. The emissivity of the aft TPS drives the amount of heat lost from the vehicle. If it is not possible to place MLI on the aft lid, then a low emissivity is desired to limit the heat lost from the aft surfaces. It is currently not clear what emissivity will be feasible on the aft lid, so several were evaluated.

The cases shown in Table 1 were run with the nominal solar angle and MLI. The properties input and resultant predicted temperatures are shown. If a relatively low emissivity of 0.3 on the aft spherical lid and spin-eject disk is feasible, then an MLI α/ε of 0.6/0.3 looks like a good choice. The predicted temperature distribution in this case is shown in Figure 5. If the afterbody must be left uncoated, such that the virgin SIRCA emissivity is used (0.9), then a slightly higher α/ε ratio of 0.5/0.2 gives a reasonable distribution, as shown in Figure 6. These figures show that the distribution pattern is very similar, although the temperature ranges differ.

Table 1. Exo-atmospheric Thermal Predictions

fore α	fore ε	aft ε	Forebody (°C)	Afterbody (°C)	OS (°C)
0.7	0.125	0.1	164	69	116
0.7	0.4	0.1	47	5	25
0.7	0.4	0.93	6	-85	-45
0.6	0.1	0.93	135	-47	30
0.8	0.1	0.93	176	-37	50
0.6	0.3	0.1	58	11	35
0.6	0.3	0.2	46	-18	15
0.6	0.3	0.3	38	-35	0
0.6	0.3	0.4	33	-47	-8
0.6	0.3	0.5	29	-56	-17
0.6	0.3	0.6	25	-64	-25
0.6	0.3	0.9	18	-79	-36
0.7	0.3	0.93	30	-75	-23
0.7	0.2	0.93	71	-62	5
0.6	0.15	0.93	84	-58	12
0.6	0.2	0.93	54	-67	-5
0.5	0.1	0.93	106	-52	25
0.5	0.2	0.93	34	-73	-20
0.5	0.3	0.93	-3	-86	-45

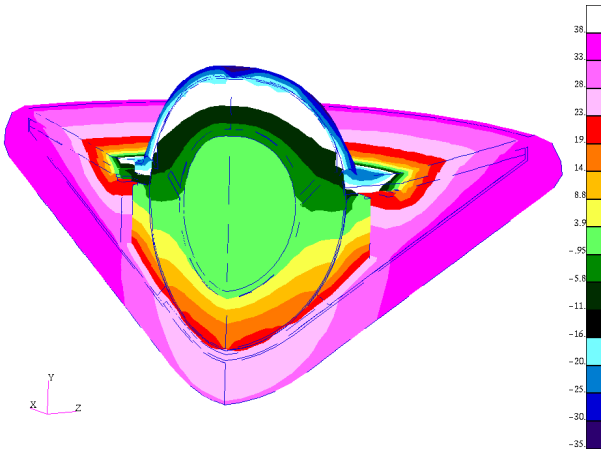

Figure 5. Exo-atmospheric distribution, MLI α/ε = 0.6/0.3, lid ε=0.3 (°C).

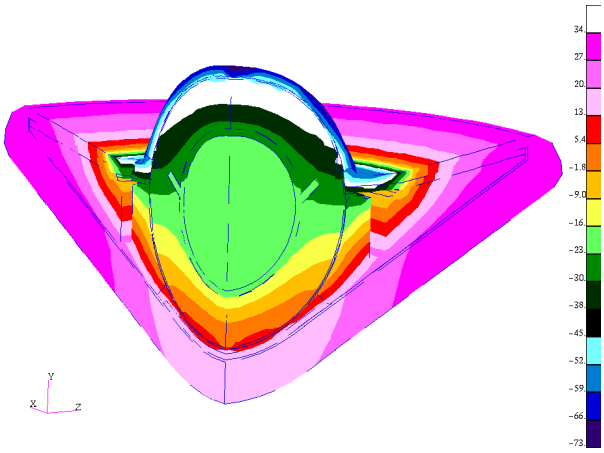

Figure 6. Exo-atmospheric distribution, MLI α/ε = 0.5/0.2, lid ε=0.9 (°C).

Results

The final prediction for exo-atmospheric cruise uses the external MLI properties of α/ε of 0.5/0.2, an exterior ε for the lid of 0.9, and adds the refinement of 3D orthotropic properties. The results are shown in Figure 7. There is a substantial smoothing of the thermal gradient due to the addition of the orthotropic properties; the overall delta across the vehicle decreases from 106°C to 64°C.

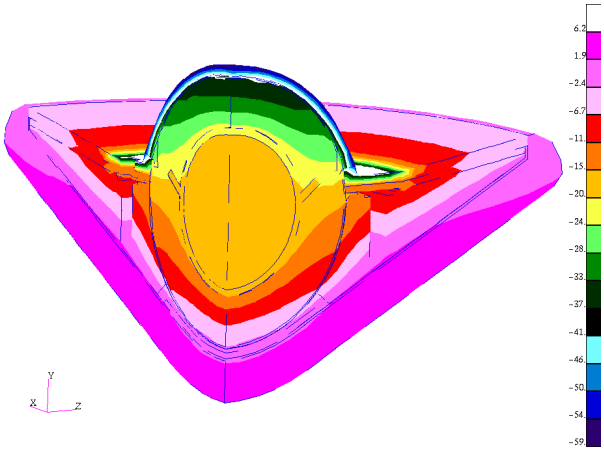

Figure 7. Exo-atmospheric prediction (°C) with orthotropic properties, MLI α/ε = 0.5/0.2, lid ε=0.9.

ENTRY PHASE RESULTS

Correlation to FIAT Model

The forebody and aftbody heating during entry dominate the thermal response of the EEV in this phase of the mission. The heating is not only a function of time but also a function of the position on the vehicle. Initial temperature predictions did not account for the loss of energy and mass due to charring, property change, blowing, gas pyrolysis, etc. The predicted temperature distribution at 70 seconds for this initial run is shown in Figure 8.

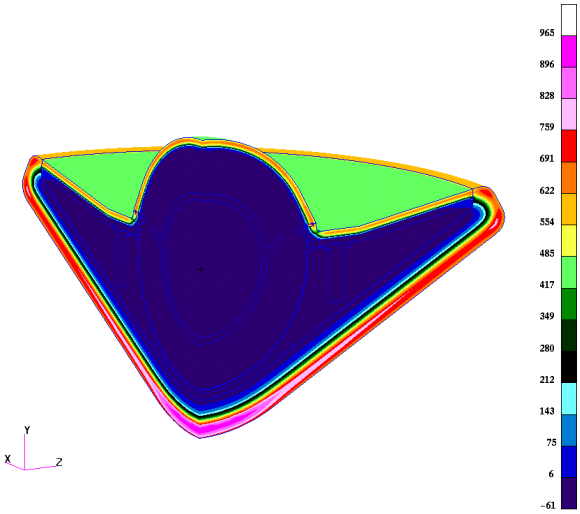

Figure 8. Temperature distribution at 70 sec (°C).

The Fully Implicit Ablation and Thermal Analysis Program (FIAT)[11] used by NASA Ames for preliminary TPS sizing accounts for all of the physical and chemical processes occurring in the TPS material. This was the primary reason FIAT was chosen as a baseline for comparison. Figure 9 shows the temperature history at the stagnation point through entry up to landing for both the PATRAN Thermal and FIAT models.

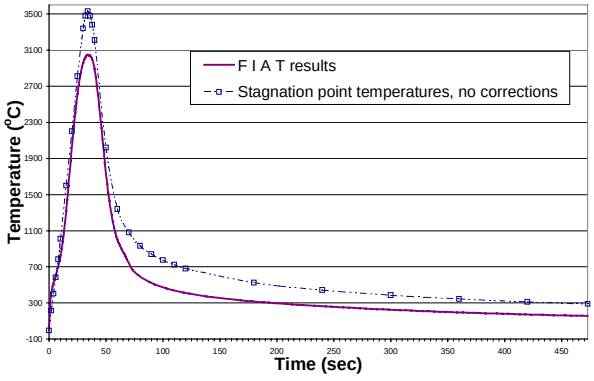

Figure 9. Stagnation point temperatures.

A maximum temperature difference of 478°C between the PATRAN and FIAT model occurred at 34 seconds. At landing (473 seconds), the temperature difference was 132°C. The temperature distribution at landing is shown in Figure 10.

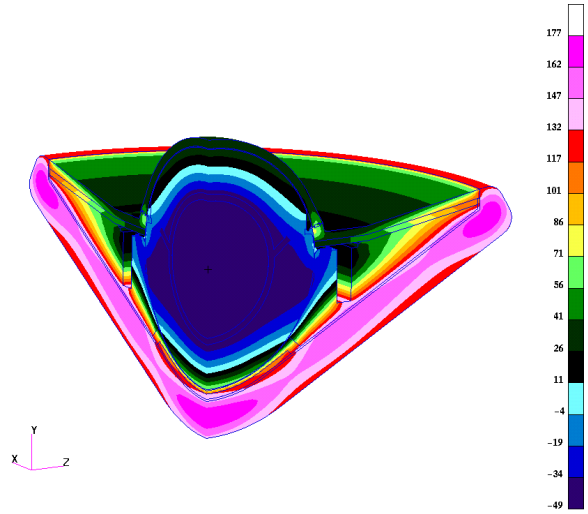

Figure 10. Temperature distribution at 473 sec (°C).

These initial results showed unsatisfactory correlation largely due to the inability of PATRAN to directly model the ablative nature of the TPS material. In order to simulate the physical and chemical processes and achieve satisfactory correlation, an engineering adjustment to the PATRAN model was needed. To correlate the data, a heat flux reduction factor and a time-varying charred material property was developed to simulate the loss of energy and mass as a result of the processes occurring during the heat pulse. The heat flux reduction factor was a simple sine function with time as the independent variable. A sine function was used to gently transition from the baseline heating profile to the maximum reduction at peak heating of 58.5%. The sine function worked very well from 25 to 45 seconds into the heat pulse. After 45 seconds, the energy loss appeared to become exponential, so after that time an exponential decay equation was used to reduce the heat. The heat flux reduction functions took the following form:

$$Q_f = \left(A\sin^4 \omega t + B\sin^2 \omega t + C\sin \omega t + D\right) * Q_o \quad (2)$$

$$Q_f = \left(Ae^{-t} + B\right) * Q_o \quad (3)$$

where t is time, Q_f is the corrected heat flux, Q_o is the actual heat flux, and ω is the frequency of the sine function. The coefficients A, B, C, and D were determined by bounding the reduction factor between a given time interval, specifying the time the maximum occurs, and specifying the maximum value of the reduction factor. This reduction factor approximation accurately simulated the response of the EEV up to about 55 seconds. After 55 seconds, the effect of charring in changing the bulk material properties becomes significant enough to diverge the results. The FIAT code models charring directly such that the vehicle loses mass and hence loses some of its ability to store energy. Therefore, to simulate the loss of mass and energy in the PATRAN model, the first two layers of elements on the forward TPS were assigned material properties of charred PICA-15 after 34 seconds (to average the time at which charring becomes significant). These two layers of elements were also given time varying, decreasing density in order to simulate the loss of mass. With the combination of the heat reduction factor and the time varying char properties, the PATRAN results showed good correlation with the FIAT model. Figure 11 shows the correlation for the stagnation point, where the temperature difference is only 7.2°C at peak heating and 12.9°C at landing.

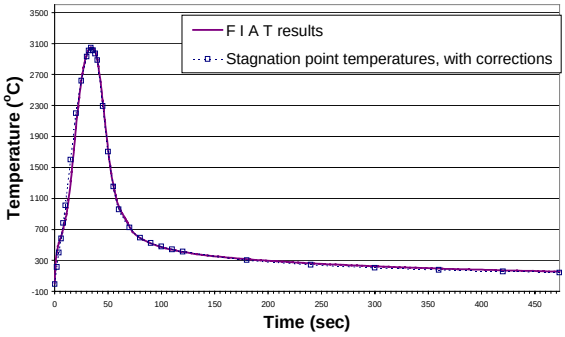

Figure 11. Correlated stagnation temperatures.

A similar correlation was obtained for interior nodes in line with the stagnation point. No adjustments to the aftbody heating were necessary, as the PATRAN and FIAT models were in good agreement. The reason for this good correlation was that the aftbody TPS material, SIRCA, was not exposed to heating rates high enough to cause significant charring.

Results

The final prediction for Earth entry uses these engineering adjustments, and adds the refinement of 3D orthotropic properties. The results are shown in Figure 12 and Figure 13. The addition of the orthotropic properties produced a noticeable increase in temperature near the outboard section of the vehicle. This increase in temperature can be attributed to the increase in the in-plane thermal conductivity, which is approximately 3 times the through-the-thickness conductivity. The increased thermal conductivity allows the energy from the heat pulse to be better distributed along the cross-section of the vehicle.

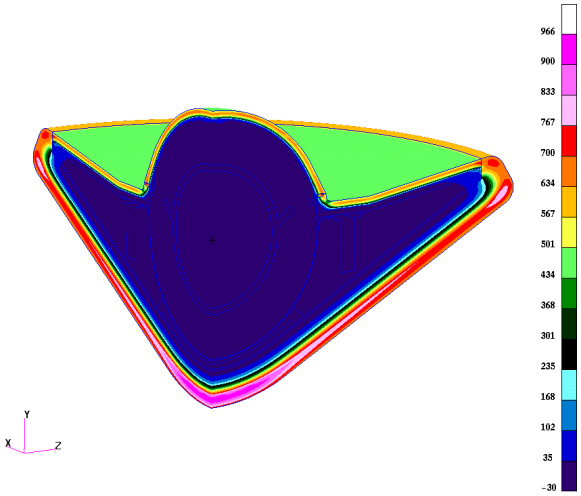

Figure 12. Final temperature prediction at 70 s (°C).

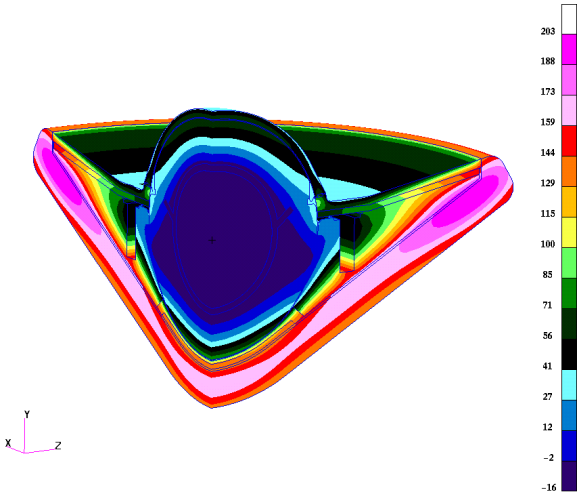

Figure 13. Final temperature prediction at 473 s (°C).

LANDED PHASE RESULTS

After landing, the vehicle begins to come to thermal equilibrium. Figure 14 shows an example analysis of the progression. By three hours after landing, the vehicle is close to thermal equilibrium and few more changes are occurring. At no time does the OS exceed the ambient temperature of 25°C. Many other cases have been run with other conditions, which vary items such as convection to ambient and which parts of the vehicle come in contact with the ground. None of these cases raise the OS temperature above 25°C.

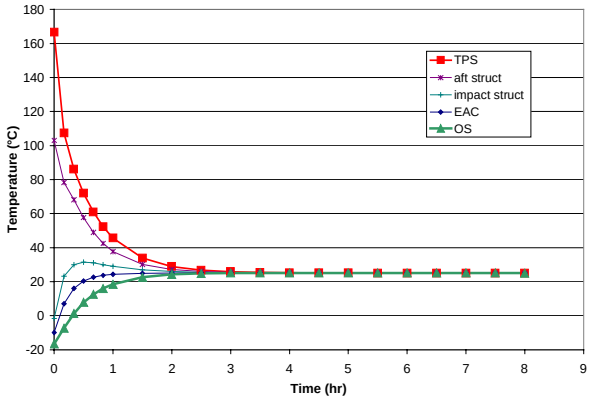

Figure 14. Transient after landing (°C).

CONCLUSIONS

A procedure was developed to perform detailed thermal analysis early in the design phase of the EEV for the Mars Sample Return mission. Results from this procedure indicate the passive design EEV was successful in maintaining all parts within their designed thermal limits. The methods for applying orbital heat flux boundary conditions were found to be efficient and flexible. Use of the Thermal Synthesizer System software to model orbital heating in a hyperbolic Earth orbit and apply those loads to the PATRAN model was successful. Exterior properties with an α/ε of roughly 0.6/0.3 were found to give an acceptable vehicle thermal distribution. A novel method for applying the entry heat loads was developed and found to be effective, resulting in good agreement between this engineering approximation and results from a full material response model. This involved a combination sine wave/exponential decrease in heating to account for blowing, and a change in properties in the outer layers to account for charring. Orthotropic material properties were successfully added to all models using complex spatial fields, and produced meaningful changes in the predicted gradients. Results in all three model phases were evaluated, and the science as well as system thermal requirements were met.

ACKNOWLEDGEMENTS

The work of YK Chen at NASA Ames in analyzing the material response during entry, which allowed correlation of this analysis, is acknowledged with deep gratitude. The work of Stephen Hughes at NASA Langley in preparing CAD models is greatly appreciated.

ACRONYMS

CAD	Computer-aided design

CV	Containment vessel
EEV	Earth Entry Vehicle
MLI	Multi-layer insulation
OS	Orbiting samples
PICA	Phenolic Impregnated Carbon Ablator
SIRCA	Silicone Impregnated Reusable Ceramic Ablator
TSS	Thermal Synthesizer System
TPS	Thermal protection system

REFERENCES

[1] R. A. Mitcheltree, S. Kellas, J. T. Dorsey, P. N. Desai and C. J. Martin, Jr., "A Passive Earth-Entry Capsule for Mars Sample Return," 7th AIAA/ASME Joint Thermodynamics and Heat Transfer Conference, Albuquerque, New Mexico, AIAA 98-2851, June 15-18, 1998.

[2] Mars Sample Return Earth Entry Vehicle Conceptual Design Assessment, NASA Langley Research Center, November 3-4, 1999, MSR EEV Project Office.

[3] Pro/ENGINEER Fundamentals Manual, Parametric Technology Corporation, Release 20.0 (June 1998).

[4] MSC/PATRAN User Manual, MacNeal-Schwendler Corporation, Version 9.0 (May 1999).

[5] User Manual, Thermal Synthesizer System, Release 6.01, Lockheed Martin Space Mission Systems, NAS9-19100, October 1997.

[6] TPSX, Thermal Protection Systems Expert and Material Properties Database, February 1998, NASA Ames Research Center (http://asm.arc.nasa.gov/tpsx/).

[7] C. W. Ohlhorst, W. L. Vaughn, P. O. Ransone, H. Tsou, "Thermal Conductivity Database of Various Structural Carbon-Carbon Composite Materials," NASA TM-4787, NASA Langley Research Center, November 1997.

[8] E. M. Silverman, "Composite Spacecraft Structures Design Guide," NASA Contractor Report 4708, Contract NAS1-19319, March 1996.

[9] D. G. Gilmore, *Satellite Thermal Control Handbook*, The Aerospace Corporation Press, El Segundo, California, 1994.

[10] J. H. Henninger, "Solar Absorptance and Thermal Emittance of Some Common Spacecraft Thermal Control Coatings," NASA Reference Publication 1121, Goddard Space Flight Center, April 1984.

[11] Y. K. Chen and F. S. Milos, "Ablation and Thermal Response Program for Spacecraft Heatshield Analysis," *Journal of Spacecraft and Rockets,* Vol. 36, No. 3, 1999, pp. 475-482.